Constant Photocurrent Method to Probe the Sub-Bandgap Absorption in Wide Bandgap Semiconductor Films

Nicol, David; Reynolds, Stephen; Barr, Kristopher; Roberts, Joseph W.; Jarman, John J.; Chalker, Paul R.

Published in:
Physica Status Solidi B: Basic Solid State Physics

DOI:
10.1002/pssb.202300470

Publication date:
2024

physica status solidi b
www.pss-b.com

Constant Photocurrent Method to Probe the Sub-Bandgap Absorption in Wide Bandgap Semiconductor Films: The Case of α-Ga_2O_3

David Nicol, Stephen Reynolds, Kristopher Barr, Joseph W. Roberts, John J. Jarman, Paul R. Chalker, and Fabien C.-P. Massabuau*

The optical absorption coefficient is one of the fundamental properties of semiconductors and is critical to the development of optical devices. Herein, a revival of the constant photocurrent method is presented to measure sub-bandgap absorption in wide bandgap semiconductor films. The method involves maintaining a constant photocurrent by continually adjusting the impinging photon flux across the energy spectrum. Under such conditions, the reciprocal of the photon flux for uniformly absorbed light is proportional to the absorption coefficient. This method is applied to α-Ga_2O_3 and reveals that it can access the absorption coefficient from 1×10^5 cm^{-1} at the band edge (5.3 eV) to 0.8 cm^{-1} close to mid-bandgap (2.7 eV). Changes in the steepness of the absorption curve in the sub-bandgap region are in excellent agreement with defect states of α-Ga_2O_3 reported by deep level transient spectroscopy, indicating that the technique shows promise as a probe of energetically distributed defect states in thin film wide bandgap semiconductors.

1. Introduction

The recent development of wide bandgap semiconductors has been pivotal in facilitating the growing demand for efficient UV photodetectors across diverse applications such as flame detection, missile tracking systems, and biochemical sensing.[1,2] Si-based devices have dominated the UV detector market for many years, despite the low Si bandgap of 1.1 eV[3] which is non-ideal for UV detector applications. UV excitation of Si results in significant phonon generation, leading to accelerated material aging and a decrease in device efficiency and operational lifetime.[4] Wide bandgap semiconductors, loosely defined as those with a bandgap energy greater than 3 eV, are naturally suited for UV photodetector applications. This category of materials encompasses ZnO, GaN, AlN, and SiC for the most mature materials,[5–8] as well as emerging materials like Ga_2O_3. Owing to a wider bandgap energy of 4.7–5.3 eV, Ga_2O_3 has gained increasing attention over recent years for its promising applications in high power electronics and solar-blind optoelectronics.[9] This polymorphic compound exists in several forms, including the thermodynamically stable β-Ga_2O_3 phase, and the metastable α-Ga_2O_3 phase. The latter is particularly attractive as it exhibits the widest bandgap (≈5.1–5.3 eV) among all phases of Ga_2O_3[10–13] and offers a wide design space for bandgap engineering through alloying with several isomorphic sesquioxides like Al_2O_3,[14] In_2O_3,[15] Fe_2O_3,[16] or Ti_2O_3.[17]

To enhance the efficiency and reliability of wide bandgap semiconductor devices, it is crucial to gain an understanding of the material's fundamental properties. Of particular relevance to the design of UV solar-blind detectors is the absorption of light by the material, quantified by the optical absorption coefficient α. Measuring the absorption coefficient as a function of photon energy at sub-bandgap photon energies reflects the presence of trap states arising from defects, or band tails associated with structural or compositional disorder.

While there are several methods for measuring the optical absorption coefficient α, few are well suited for accurate measurements within the bandgap. Optical transmission is the most common method to measure the absorption coefficient and provides good accuracy for energies near the bandgap of the

D. Nicol, K. Barr, F. C.-P. Massabuau
Department of Physics
University of Strathclyde
Glasgow G4 0NG, UK
E-mail: david.nicol@strath.ac.uk

S. Reynolds
School of Science and Engineering
University of Dundee
Dundee DD1 4HN, UK

J. W. Roberts, P. R. Chalker
School of Engineering
University of Liverpool
Liverpool L69 3GH, UK

J. J. Jarman
Department of Materials Science and Metallurgy
University of Cambridge
Cambridge CB3 0FS, UK

The ORCID identification number(s) for the author(s) of this article can be found under https://doi.org/10.1002/pssb.202300470.

DOI: 10.1002/pssb.202300470

material. However, the method lacks accuracy in the sub-bandgap region, as transmission is naturally high thus limiting the ability of the detector to sense subtle variations in transmittance and small experimental inaccuracies begin to dominate the apparent absorption measurement. Photothermal deflection spectroscopy is the standard measurement technique when measuring the absorption coefficient at sub-bandgap energies,[18] and has been applied to investigate β-Ga_2O_3 films.[19]

An alternative approach to obtain an accurate measurement of the absorption coefficient in the sub-bandgap range is the constant photocurrent method (CPM). This photoconductive technique involves continually adjusting the photon flux incident on the material to maintain a constant photocurrent across the energy spectrum.[20] Under such conditions, the reciprocal of the photon flux is proportional to the absorption coefficient. This method is well established in the study of sub-bandgap absorption in amorphous Si[21–23] but has been largely overlooked for wide bandgap semiconductors. In an early application, Vaněček et al. mapped the absorption spectrum of hydrogenated Si extending into the mid-gap region.[22] Other than Si, CPM has been used in CdSe,[24] $CuGaSe_2$,[25] and AlGaN/GaN heterostructures which to our knowledge is the material with the widest bandgap investigated so far using CPM.[26]

Studying sub-bandgap absorption can be challenging due to the requirement of a large enough optical signal over a broad spectral range to generate a photocurrent. Deuterium and xenon broadband light sources are available commercially and yield a spectrum over a broad range. However, these sources are still relatively weak in the sub-bandgap region of wide bandgap semiconductors. Furthermore, spectrally resolving the broad emission of these sources may induce parasitic second order diffraction effects. In this study, we present an adapted experimental setup by implementing a broad range of light-emitting diodes (LEDs) in place of a broadband light source to conduct CPM acquisition in wide bandgap semiconductors. We illustrate the methodology by characterizing the sub-bandgap absorption in α-Ga_2O_3 thin films ($E_g \approx 5.3$ eV), and combine the CPM data with optical transmission measurements to obtain an experimental determination of the absorption coefficient α measured from 2.7 to 5.3 eV, i.e., covering half of the α-Ga_2O_3 bandgap.

2. Theoretical Background

Photoconduction is the process whereby the conductivity σ of a material increases under photon illumination. Under light illumination, photoconductivity $\Delta\sigma$ can be expressed as

$$\Delta\sigma = q(\Delta n\mu_n + \Delta p\mu_p) \tag{1}$$

where q is the charge of the carrier, Δn (Δp) is the excess free electron (hole) density generated by the incident photons, and μ_n (μ_p) is the electron (hole) mobility.[27] Equation (1) shows that the photoconduction process is dependent on carrier mobility, which is itself influenced by the effective mass of the electrons and holes. In wide bandgap semiconductors, the effective mass of the electrons is typically lower than that of the holes, resulting in greater electron mobility (e.g., $\frac{\mu_n}{\mu_p} \sim 100$ for GaN[28] and SiC-4H[29] and $\frac{\mu_n}{\mu_p} \sim 200$ are predicted for Ga_2O_3[30]). Under the conditions of electron-dominated transport, Equation (1) can be simplified to

$$\Delta\sigma = q\Delta n\mu_n \tag{2}$$

Δn is the product of the carrier-generation rate G and the free electron lifetime τ_n, the mean time spent by excess (photogenerated) electrons in the conduction band before they recombine.

$$\Delta n = G\tau_n \tag{3}$$

The value of τ_n depends upon the recombination mechanism prevailing. It is often found to be a function of photon flux, as reflected in a sub- or supralinear dependence of photocurrent on photon flux measurements in materials such as Ga_2O_3,[31,32] GaN,[33] and ZnO.[34] This nonlinearity stems from complex recombination mechanisms, which may involve bimolecular or trap-mediated carrier kinetics. While recombination processes are an important area of study in semiconductor materials, our focus in this article is on the use of photoconductivity in a spectroscopic role, as developed below.

Substituting Equation (3) into (2) gives

$$\Delta\sigma = Gq\tau_n\mu_n \tag{4}$$

The average photocarrier generation rate G is defined as[27]

$$G = \eta\Phi(1-R)\frac{1-\exp(-\alpha d)}{d} \tag{5}$$

where η is the quantum efficiency, Φ is the incident photon flux, R is the film reflectance, α is the absorption coefficient of the film, and d is the film thickness. The situation for various values of αd is illustrated in **Figure 1**. In the case of weak optical absorption typical for sub-bandgap excitation, that is, where $\alpha d \ll 1$, the generation rate is uniform throughout the film, and Equation (5) can be approximated as

$$G \approx \eta\Phi(1-R)\alpha \tag{6}$$

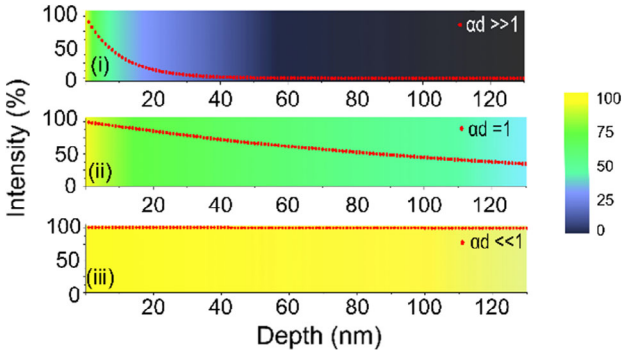

Figure 1. Transmitted light intensity (incident from the left) versus depth in a 130 nm thick film, described by the Beer Lambert law: i) $\alpha d \gg 1$: incident light is strongly absorbed at the surface of the film; ii) $\alpha d = 1$: 67% of the light is absorbed within the film; and iii) $\alpha d \ll 1$: light absorption is small and uniform throughout the film, giving a constant generation rate and carrier lifetime.

Substituting Equation (6) into (4) gives

$$\Delta\sigma = \eta\Phi(1-R)\alpha q\tau_n\mu_n \tag{7}$$

Under the reasonable assumption that η, μ_n, and R do not vary significantly with incident photon energy, as is typically the case for sub-bandgap excitation, Equation (7) indicates that the absorption coefficient α is a function of $\Delta\sigma$, Φ, and τ_n. Furthermore, if we actively maintain a constant photocurrent by adjusting Φ at each photon energy, the quasi-Fermi levels are fixed, which in turn maintains a constant τ_n. Thus, under the constant photocurrent conditions, Equation (7) reduces to

$$\alpha(E_{ph}) = \frac{\text{Constant}}{\Phi(E_{ph})} \tag{8}$$

where E_{ph} is the photon energy. Equation (8) shows that by recording the photon flux $\Phi(E_{ph})$ required to maintain a constant photocurrent versus energy, we obtain a relative measure of the absorption coefficient α, given that we maintain a uniform generation rate throughout the sample thickness ($\alpha d \ll 1$). The CPM spectrum may be calibrated by overlapping with the optical absorption spectrum in the region where both are approximately valid ($\alpha d \leq 1$).

The absorption coefficient $\alpha(E_{ph})$ is determined by the sum of all the permitted transitions between occupied and empty electron states. It follows that α and the density of states (DOS), defined as the number of states per unit volume per unit energy, are related. During the CPM experiment, sweeping from lower to higher E_{ph} elicits transitions from deeper filled states in the bandgap, which continue to accrue with increasing photon energy as additional filled states are brought into play. Therefore, CPM can be used as a DOS spectroscopy technique of localized states, provided 1) the states are filled, i.e., below the Fermi level; 2) the conduction band edge is sharp relative to the distribution of the localized states in the bandgap; and 3) thermally assisted transitions are ignored.[23] The DOS $g(E)$, where $E = E_C - E_{ph}$, is then proportional to $\frac{d\alpha(E_{ph})}{dE_{ph}}$.[35] We consider how CPM might be used to identify specific defect states in Ga_2O_3 later in this work.

3. Experimental Section

3.1. Sample Preparation

In this study, we used an unintentionally doped 130 nm thick α-Ga_2O_3 film grown on *c*-plane Al_2O_3 by plasma enhanced atomic layer deposition. Further details on the growth of the sample are detailed in ref. [12]. X-ray diffractograms revealed an intense reflection near $2\theta = 40.25°$ which corresponded to the α-Ga_2O_3 0006 reflection. Additional reflections at lower angles indicated additional phase inclusions from κ-Ga_2O_3 as was also observed by transmission electron microscopy.[12] The films were processed into photodetector structures by depositing interdigitated Ti (20 nm)/Au (80 nm) metal electrodes to produce Ohmic contacts.[36,37]

3.2. UV–Vis Spectrophotometry

Optical transmission measurements were obtained using a Shimadzu UV-2600 UV–vis spectrophotometer equipped with an integrating sphere. The absorption coefficient spectrum was obtained from the Beer Lambert law.

$$\alpha(E_{ph}) = \frac{1}{d}\ln\left(\frac{1}{T}\right) \tag{9}$$

where d is the film thickness and T is the transmittance.

3.3. CPM Setup

Optical excitation across the energy spectrum was generated using a series of LEDs covering photon energies from ≈2.7 to 5.2 eV (corresponding to wavelengths from 240 to 460 nm) detailed in **Table 1**. A DC power supply controlled the LED driving current between 1 and 50 mA. While considered monochromatic, the emission spectrum of LEDs could be relatively broad, and shift with temperature or operating current. To select a narrower wavelength range, the output from the LED was spectrally resolved using a Solar Laser Systems ML44 high aperture compact monochromator with a diffraction grating of 1200 lines mm^{-1} blazed at 270 nm, with its slits set to achieve a spectral bandpass of (3 ± 1) nm. An optic fiber was used to direct the light to the sample, positioned 5 mm from the exit of the optic fiber at ≈45° incidence. Fine control of photon flux was achieved by adjusting the LED current. Close to the bandgap of α-Ga_2O_3 (≈240–270 nm) neutral density filters were required for coarse attenuation of the photon flux. The sample photocurrent was measured at a bias of 10 V using a Keithley 6487 Picoammeter on a Signatone probe station. The optical power incident on the sample was measured using a Thorlabs PM100 power meter unit with a coupled S130VC Si photodiode. The experimental set up is illustrated in **Figure 2**.

3.4. CPM Procedure

The first step of the approach was to choose a value of photocurrent to be kept constant throughout the experiment, referred to as the CPM reference value. This value must be sufficiently high to

Table 1. Details of LEDs used for the CPM experiment, supplied from Thorlabs.

Part number	Wavelength [nm]	Nominal power [mW]	Bandwidth [nm]	Viewing half angle [°]
LED 465E	465	20	25	8
LED 450L	450	7	20	20
LED 430L	430	8	20	22
LED 405E	405	8.4	15	5
LED 375L	375	1	10	20
LED 325W2	325	1.7	11	114
LED 275J	275	1.6	11	7.5
LED 250J	250	1	12	7.5

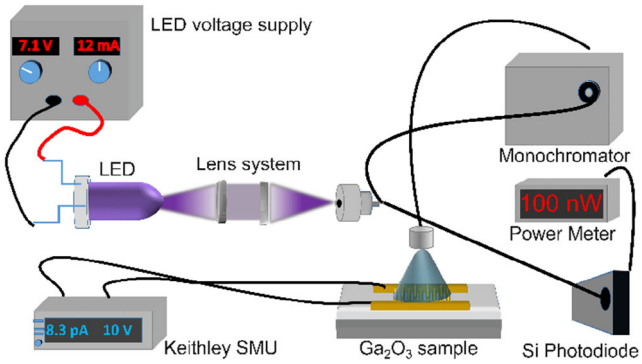

Figure 2. CPM experimental set-up.

give a good signal-to-noise ratio but remain low so that the photocurrent must not greatly exceed the sample dark current; otherwise, the occupancy of states in the gap close to the Fermi level would be modified which in turn would yield an inaccurate value of the absorption coefficient. The dark current in our device was typically 1 pA at room temperature, and a CPM reference value of 7.8 pA was chosen. The validity of the CPM reference was demonstrated over a range of 7.8–117 pA, highlighted in **Figure 3**. Due to the limited power of the LEDs in the low absorption region, it was not possible to maintain a high CPM reference current in that region. Therefore, a CPM reference value of 7.8 pA was selected to probe deeper into the bandgap of the material. Furthermore, as Ga_2O_3 was reported to have a low conduction band DOS, the possibility of excitation to a second transport band in the CB was considered. Peelaers et al. demonstrated theoretically that when the carrier density exceeds $\approx 10^{19}$ cm^{-3}, carriers are excited to additional conduction bands.[38] In this work, our sample is non-intentionally doped, and the low photocurrent used results in a carrier density orders of magnitude lower than predicted by Peelaers, therefore, this effect is unlikely.

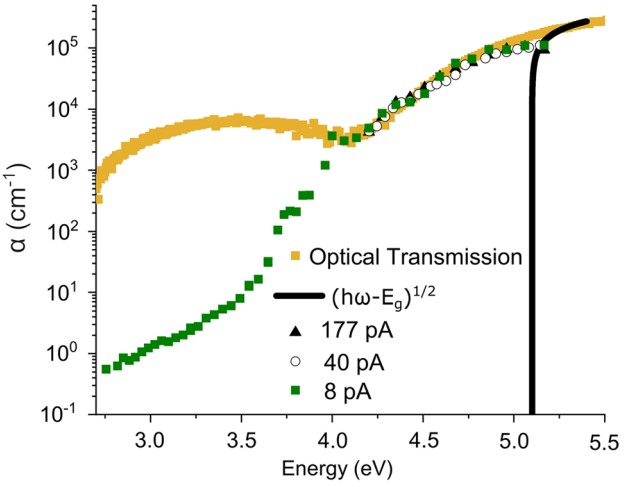

Figure 3. Absorption coefficient spectra of α-Ga_2O_3 obtained via CPM using different CPM reference currents (8 pA [green squares], 40 pA [white circles], and 177 pA [black triangles]) and optical transmission methods [gold]. The black line indicates how the absorption coefficient should scale in a direct bandgap semiconductor for a perfect crystal.[41]

The longest wavelength, 465 nm LED, was first selected and scanned spectrally from 470 to 450 nm in 3 nm steps using the monochromator. The initial setting of the CPM reference value was carried out at 470 nm. The optical flux was then measured using the power meter. The wavelength selection in the monochromator was then decreased by 3 nm and the LED driving current was adjusted so that the sample photocurrent remained matched to the CPM reference value within 5%, with the optical flux measured at each wavelength increment. This process was repeated with the same LED until the CPM reference value could not be reached (i.e., when the chosen wavelength was too far from the LED peak wavelength to generate sufficient photocurrent). The light source was then switched to the LED next in line, here a 450 nm LED, and the process repeated. At the crossover wavelength between LEDs, spectral overlap was required to generate a continuous spectrum. The final two measurements of the 465 nm LED and the first two measurements with the 450 nm LED were matched and the spectra overlapped. This process was repeated with the complete series of LEDs until reaching bandgap excitation, here 240 nm. As presented in the theoretical background section, plotting the reciprocal of the optical flux versus photon energy results in a value proportional to the absorption coefficient α (Equation (8))—the proportionality lies with the constants outlined in Equation (7). To remove the proportionality factor, the CPM spectrum is normalized to the absorption coefficient in the high absorption region (i.e., near-bandgap energy) obtained from the optical transmission measurements. This was achieved by overlapping the CPM and optical transmission measurements where both were approximately valid at $\alpha d \leq 1$.

4. Results and Discussion

Figure 3 compares the experimental absorption coefficient versus photon energy obtained by CPM and optical transmission for our α-Ga_2O_3 sample. As explained in Experimental Section, the CPM spectrum was overlapped with the high absorption region in the optical transmission spectrum at ≈4.7 eV (corresponding to $\alpha d = 1$ condition). The requirement for the scaling of the CPM spectrum using the absolute values of α from the optical absorption spectrum is rooted in Equation (8), which shows that plotting the reciprocal of the photon flux versus photon energy yields a value proportional to the absorption coefficient. In this spectral region, it becomes increasingly difficult to measure the absorptance using conventional optical spectrophotometry, and this is evident in Figure 3, where we believe that the apparent increase in absorptance arises from thin-film interference effects. In principle, these reflections could excite additional carriers into the conduction band which would show as a series of fringes in the obtained CPM absorption curve. Typically, this is accounted for by simultaneously measuring the transmitted light through the sample, often referred to as "absolute CPM".[39] However, here we observed no sign of interference fringes in the measured CPM absorption spectra (Figure 3); therefore, the absolute CPM technique was deemed unnecessary.

In principle, carrier transitions yielding either a free electron or free hole can give rise to an increase in carrier photocurrent, leading to a potentially complex situation. Fortunately, the hole

mobility is low in Ga_2O_3. Calculations of the band structure indicate that the valence band is comprised of oxygen (O) 2p orbitals, giving a flat E–k relationship and a low effective mass Additionally, due to strong electron–hole coupling, holes will tend to become self-trapped at O sites due to local lattice distortions.[40] We therefore believe it is reasonable to suppose that electron transport dominates the measured photocurrent, due to transitions from filled states below the Fermi level to the conduction band.

The CPM spectrum exhibits a number of features, and is divided into four regions for the purpose of discussion. These are highlighted in **Figure 4**a and the corresponding electronic transitions are schematized in Figure 4b. It should be noted here that we have measured the dark current activation energy for our samples, which lie in the range of 0.6–1.0 eV, placing the dark Fermi level at a similar energy level below the conduction band edge. This indicates that under CPM conditions, states from the valence band to above mid-gap are fully occupied, and are therefore accessible.

Region (i) spans the energy range greater than 5.1 eV and represents the high absorption region of the film. Given that α-Ga_2O_3 exhibits a bandgap energy of 5.1 eV, as determined here from the optical transmission and in line with previous reports;[10–12] in that region, we expect carriers to be excited to the conduction band from all filled states below the Fermi level including excitation from valence band to conduction band. If the material were a perfect direct bandgap semiconductor, with no states in the bandgap, the energy-dependent absorption coefficient should scale with the square root of the photon energy above the bandgap.[41] We would then expect the absorption coefficient to fall rapidly to zero at energies below the bandgap energy —as illustrated by the black line in Figure 3. If states extending from the valence band edge into the bandgap are present, the absorption coefficient will fall less rapidly as the photon energy is gradually reduced below the bandgap energy. This is observed in region (ii), spanning energies between 4 and 5.1 eV. Here, we see a pronounced broadening of the absorption edge. In bulk single-crystal β-Ga_2O_3, the extension of the band edge into the sub-bandgap region has been measured by Hao et al. using photothermal deflection spectroscopy, in which their results were characterized by a characteristic slope energy of 100–200 meV.[19] In our work, we obtain a value of 430 meV which is significantly wider, attributed to structural disorder, defect incorporation, and phase inclusions, which we know are present in this film.[12,36] An important element in interpreting the absorption coefficient versus photon energy curve is to deduce which set of states (empty, filled, or both) determines its "shape" in each region. Generally, the broader (or less steeply varying) of the two will be the dominant process in the convolution. In the case of Ga_2O_3, it seems likely that the conduction band edge is a relatively sharp energy probe, with a narrow, low density of tail states. If significant tail states were present, they would reduce electron mobility by multiple trapping—repeatedly immobilizing carriers in shallow states until they are reemitted to the conduction band. Since mobilities of $\approx 100\,cm^2\,V^{-1}\,s^{-1}$ have been measured in Ga_2O_3 at room temperature,[42] and values of $200–300\,cm^2\,V^{-1}\,s^{-1}$ are predicted,[43–45] and controlled n-type doping with shallow donors is possible, there is no support for conduction band tail states being responsible for the transitions in region (ii). We therefore believe this broad absorption in Ga_2O_3, extending between 4.0 and 5.1 eV, is associated with filled states adjacent to the valence band.

Region (iii), which covers energies from 3.6 to 4 eV, highlights the effectiveness of the CPM approach for obtaining the absorption coefficient in the sub-bandgap region. As previously discussed, the accuracy of the optical transmission measurements diminishes as the transmitted light is maximized and the detector cannot accurately measure relatively small intensity variations against a large transmitted background. In contrast, CPM reveals two orders of magnitude decrease in the absorption coefficient, from $3 \times 10^3\,cm^{-1}$ at 4 eV to $16\,cm^{-1}$ at 3.6 eV. Furthermore, we observe that the slope differs from that of region (ii) in terms of steepness, which could imply that electrons are being excited from states with different absorption characteristics than region (ii). Given that the photon energy is here much lower than the bandgap energy, it seems reasonable to infer that absorption in region (iii) corresponds to transitions of electrons from filled states below the Fermi level to the conduction band. Here, we refer to the literature as a reference to defect states in the bandgap of α-Ga_2O_3.[46] Due to the energy range, we are looking at defect levels which would reside between 3.6 and 4.0 eV below the conduction band. Theoretical calculations suggest that isolated gallium vacancies (V_{Ga}) reside around 3.5 eV below the conduction band edge in α-Ga_2O_3.[47] Gallium interstitials (Ga_i)

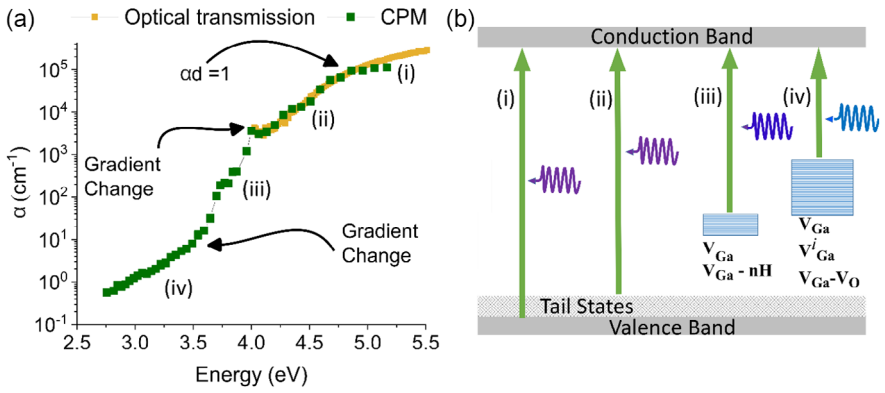

Figure 4. a) Absorption coefficient obtained via CPM, and b) corresponding band diagram illustrating electron transitions contributing to the measured conductivity.

and substitutional gallium (Ga_O) are predicted to have activation energies in the same energy region; however, both defects exhibit high formation energies and, therefore, are not expected to be the responsible defect.[47,48] This was supported experimentally by deep-level optical spectroscopy revealing V_{Ga}-related defect states located ≈ 3.5 eV below the conduction band.[49,50] Further work from Polyakov et al. suggested H-decorated complexes exhibit defect levels situated 3.8–3.9 eV below the conduction band edge,[51] and luminescence studies have associated 3.8 eV luminescence with H-decorated V_{Ga}.[52] The low formation energy of the H-decorated V_{Ga} compared to isolated V_{Ga} suggests that it is the most probable form of the defect.[53] Here, we must note that if a discrete set of traps were responsible for the transition, this would be reflected as a series of steps in the absorption spectrum, with each step associated with the activation energy of that discrete level. Figure 4a is more reflective of an exponentially distributed set of states within the bandgap. We therefore tentatively ascribe an exponential distribution of V_{Ga}–nH complexes as the origin of the absorption in region (iii). We finally point out that the transitions in region (iii) will be a convolution of transitions from filled states in regions (iii) and (iv).

Lastly, region (iv) shows that the absorption coefficient decrease extends further, from 16 cm^{-1} at 3.6 eV to 0.8 cm^{-1} at 2.7 eV, with a different slope than for regions (ii) and (iii). Again, this region is masked on the optical transmission measurements. Following a similar reasoning as for region (iii), we interpret absorption in that region as resulting from transitions from filled states below the Fermi level to the conduction band. To interpret the origin of this region in absorption, we should look for defect states residing between 2.7 and 3.6 eV below the conduction band. As previously mentioned, isolated V_{Ga} resides around 3.5 eV below the conduction band edge; however, it is observed in the optical deep-level transient spectroscopy literature that di-vacancies of V_{Ga} and V_O (V_{Ga}–V_O) add additional energetic states distributed between ≈ 2.0 and 3.5 eV below the conduction band, depending on the charge state of each isolated defect.[46,48] From a theoretical perspective, Varley et al. revealed the possibility of isolated V_{Ga} which have relaxed to occupy interstitial sites, with energetic levels calculated to be in the range of 2.1–3.3 eV below the conduction band, with the energy level determined by the charge state of the defect.[53] Therefore, we tentatively interpret region (iv) as arising from an exponentially distributed set of states related to V_{Ga}-related defects involving $V_{Ga}-V_O$ complexes, isolated V_{Ga} or relaxed V_{Ga} occupying interstitial sites.

5. Conclusion

We present a revival of the CPM as a means of measuring the absorption coefficient at sub-bandgap energies in wide bandgap semiconductor films and demonstrate its application on α-Ga_2O_3. The study combines optical transmission measurements and CPM data to quantify the absorption coefficient spanning from 0.8 to 10^5 cm^{-1} over an energy range of 2.7–5.3 eV. The absorption spectrum was dissected into four distinct regions which highlight the different electronic transitions leading to photocurrent in the material. These regions reveal contributions from band-to-band transitions (region (i)), band tails (region (ii)), defect-mediated transitions which we tentatively ascribe to an exponentially distributed set of states related to isolated V_{Ga} and V_{Ga}-nH complexes (region (iii)) and V_{Ga}–V_O divacancies, and relaxed V_{Ga} occupying interstitial sites (region (iv)). This study demonstrates that CPM is an effective method for quantifying the sub-bandgap absorption coefficient as well as investigating deep trap states in thin films.

Acknowledgements

The authors acknowledge the support from the Royal Society (grant no. RGS/R1/201236) and the Engineering and Physical Sciences Research Council (grant nos. EP/T517938/1 and EP/V034995/1).

Conflict of Interest

The authors declare no conflict of interest.

Data Availability Statement

The data that support the findings of this study are openly available in Pure Portal at https://doi.org/10.15129/6e23e883-8da6-49f0-aa15-4875e4c98f21.

Keywords

defect states, gallium oxide, photocurrents, photoelectrical characterizations, wide bandgap semiconductors

Received: October 13, 2023
Revised: February 5, 2024
Published online:

[1] X. Lu, X. Tong, Z. Zhang, F. Liang, L. Liang, L. Luo, Y. Wu, *Adv. Funct. Mater.* **2019**, *29*, 1806006.
[2] L. Sang, M. Liao, M. Sumiya, *Sensors* **2013**, *13*, 10482.
[3] M. Okil, M. S. Salem, T. M. Abdolkader, A. Shaker, *Silicon* **2022**, *14*, 1895.
[4] H. Zhou, J. Zhang, C. Zhang, Q. Feng, S. Zhao, P. Ma, Y. Hao, *J. Semicond.* **2019**, *40*, 011803.
[5] Y. K. Fang, S.-B. Hwang, K.-H. Chen, C.-R. Liu, M.-J. Tsai, L.-C. Kuo, *IEEE Trans. Electron Devices* **1992**, *39*, 292.
[6] X. H. Xie, Z. Z. Zhang, C. X. Shan, H. Y. Chen, D. Z. Shen, *Appl. Phys. Lett.* **2012**, *101*, 081104.
[7] H. Zhu, C. X. Shan, B. Yao, B. H. Li, J. Y. Zhang, D. X. Zhao, D. Z. Shen, X. W. Fan, *J. Phys. Chem. C* **2008**, *112*, 20546.
[8] R. McClintock, A. Yasan, K. Minder, P. Kung, M. Razeghi, *Appl. Phys. Lett.* **2005**, *87*, 241123.
[9] S. J. Pearton, J. Yang, P. H. Cary, F. Ren, J. Kim, M. J. Tadjer, M. A. Mastro, *Appl. Phys. Rev.* **2018**, *5*, 011301.
[10] D. Shinohara, S. Fujita, *Jpn. J. Appl. Phys.* **2008**, *47*, 7311.
[11] H. Sun, K.-H. Li, C. G. T. Castanedo, S. Okur, G. S. Tompa, T. Salagaj, S. Lopatin, A. Genovese, X. Li, *Cryst. Growth Des.* **2018**, *18*, 2370.
[12] J. W. Roberts, P. R. Chalker, B. Ding, R. A. Oliver, J. T. Gibbon, L. A. H. Jones, V. R. Dhanak, L. J. Phillips, J. D. Major, F. C.-P. Massabuau, *J. Cryst. Growth* **2019**, *528*, 125254.
[13] V. D. Wheeler, N. Nepal, D. R. Boris, S. B. Qadri, L. O. Nyakiti, A. Lang, A. Koehler, G. Foster, S. G. Walton, C. R. Eddy, D. J. Meyer, *Chem. Mater.* **2020**, *32*, 1140.

[14] R. Jinno, C. S. Chang, T. Onuma, Y. Cho, S.-T. Ho, D. Rowe, M. C. Cao, K. Lee, V. Protasenko, D. G. Schlom, D. A. Muller, H. G. Xing, D. Jena, *Sci. Adv.* **2021**, *7*, eabd5891.
[15] K. Kaneko, K. Uno, R. Jinno, S. Fujita, *J. Appl. Phys.* **2022**, *131*, 090902.
[16] S. Fujita, K. Kaneko, *J. Cryst. Growth* **2014**, *401*, 588.
[17] A. Barthel, J. Roberts, M. Napari, M. Frentrup, T. Huq, A. Kovács, R. Oliver, P. Chalker, T. Sajavaara, F. Massabuau, *Micromachines* **2020**, *11*, 1128.
[18] W. B. Jackson, N. M. Amer, A. C. Boccara, D. Fournier, *Appl. Opt.* **1981**, *20*, 1333.
[19] S. Hao, M. Hetzl, V. F. Kunzelmann, S. Matich, Q. Sai, C. Xia, I. D. Sharp, M. Stutzmann, *Appl. Phys. Lett.* **2020**, *116*, 092102.
[20] S. Reynolds, M. Brinza, M. L. Benkhedir, G. J. Adriaenssens, in *Springer Handbook of Electronic and Photonic Materials* (Eds: S. Kasap, P. Capper), Springer International Publishing, Cham **2017**, p. 151–173.
[21] M. Vaněček, J. Kočka, A. Poruba, A. Fejfar, *J. Appl. Phys.* **1995**, *78*, 6203.
[22] M. Vaněček, J. Kočka, J. Stuchlík, A. Třiska, *Solid State Commun.* **1981**, *39*, 1199.
[23] C. Main, S. Reynolds, I. Zrinščak, A. Merazga, *J. Non-Cryst. Solids* **2004**, *338–340*, 228.
[24] J. Kaur, S. K. Tripathi, in *Determination of Density of States Using Constant Photocurrent Method in Nc-CdSe:Sn Thin Films*, Indian Institute of Technology, Bombay, Mumbai, India **2013**, pp. 224–225.
[25] A. Meeder, D. F. Marrón, A. Rumberg, M. Lux-Steiner, V. Chu, J. P. Conde, *J. Appl. Phys.* **2002**, *92*, 3016.
[26] M. Niehus, R. Schwarz, S. Koynov, M. Heuken, D. Meister, B. K. Meyer, *Diamond Relat. Mater.* **2001**, *10*, 1331.
[27] R. H. Bube, in *Photoelectronic Properties of Semiconductors*, Cambridge University Press, New York **1992**.
[28] T. T. Mnatsakanov, M. E. Levinshtein, L. I. Pomortseva, S. N. Yurkov, G. S. Simin, M. Asif Khan, *Solid-State Electron.* **2003**, *47*, 111.
[29] T. Kimoto, in *Wide Bandgap Semiconductor Power Devices*, Elsevier, Duxford **2019**, pp. 21–42.
[30] C. Ma, Z. Wu, Z. Jiang, Y. Chen, W. Ruan, H. Zhang, H. Zhu, G. Zhang, J. Kang, T.-Y. Zhang, J. Chu, Z. Fang, *J. Mater. Chem. C* **2022**, *10*, 6673.
[31] S. Zhou, X. Peng, H. Liu, Z. Zhang, L. Ye, H. Li, Y. Xiong, L. Niu, F. Chen, L. Fang, C. Kong, W. Li, X. Yang, H. Zhang, *Opt. Mater. Express* **2022**, *12*, 327.
[32] Y. Wang, S. Li, J. Cao, Y. Jiang, Y. Zhang, W. Tang, Z. Wu, *Mater. Des.* **2022**, *221*, 110917.
[33] E. Akar, I. Dimkou, A. Ajay, E. Robin, M. I. Den Hertog, E. Monroy, *ACS Appl. Nano Mater.* **2023**, *6*, 12792.
[34] A. A. Bahishti, A. Majid, *Adv. Nan. Res.* **2017**, *1*, 23.
[35] K. Pierz, H. Mell, J. Terukov, *J. Non-Cryst. Solids* **1985**, *77–78*, 547.
[36] J. Moloney, O. Tesh, M. Singh, J. W. Roberts, J. C. Jarman, L. C. Lee, T. N. Huq, J. Brister, S. Karboyan, M. Kuball, P. R. Chalker, R. A. Oliver, F. C.-P. Massabuau, *J. Phys. D: Appl. Phys.* **2019**, *52*, 475101.
[37] F. Massabuau, D. Nicol, F. Adams, J. Jarman, J. Roberts, A. Kovács, P. Chalker, R. Oliver, *J. Phys. D: Appl. Phys.* **2021**, *54*, 384001.
[38] H. Peelaers, C. G. Van de Walle, *Appl. Phys. Lett.* **2017**, *111*, 182104.
[39] A. Fejfar, A. Poruba, M. Vaněček, J. Kočka, *J. Non-Cryst. Solids* **1996**, *198–200*, 304.
[40] J. B. Varley, A. Janotti, C. Franchini, C. G. Van de Walle, *Phys. Rev. B* **2012**, *85*, 081109.
[41] J. I. Pankove, in *Optical Processes in Semiconductors*, Dover Publications Corporation, New York **1975**.
[42] Z. Feng, A. F. M. Anhar Uddin Bhuiyan, M. R. Karim, H. Zhao, *Appl. Phys. Lett.* **2019**, *114*, 250601.
[43] Y. Kang, K. Krishnaswamy, H. Peelaers, C. G. Van De Walle, *J. Phys.: Condens. Matter* **2017**, *29*, 234001.
[44] M. Higashiwaki, K. Sasaki, A. Kuramata, T. Masui, S. Yamakoshi, *Appl. Phys. Lett.* **2012**, *100*, 013504.
[45] A. Sharma, U. Singisetti, *Appl. Phys. Lett.* **2021**, *118*, 032101.
[46] Z. Wang, X. Chen, F.-F. Ren, S. Gu, J. Ye, *J. Phys. D: Appl. Phys.* **2021**, *54*, 043002.
[47] M. Uddin Jewel, S. Hasan, I. Ahmad, *Comput. Mater. Sci.* **2023**, *218*, 111950.
[48] M. E. Ingebrigtsen, A. Kuznetsov, B. G. Svensson, G. Alfieri, A. Mihaila, U. Badstübner, A. Perron, L. Vines, J. B. Varley, *APL Mater.* **2019**, *7*, 022510.
[49] A. Y. Polyakov, N. B. Smirnov, I. V. Shchemerov, E. B. Yakimov, S. J. Pearton, C. Fares, J. Yang, F. Ren, J. Kim, P. B. Lagov, V. S. Stolbunov, A. Kochkova, *Appl. Phys. Lett.* **2018**, *113*, 092102.
[50] E. Farzana, E. Ahmadi, J. S. Speck, A. R. Arehart, S. A. Ringel, *J. Appl. Phys.* **2018**, *123*, 161410.
[51] A. Y. Polyakov, V. I. Nikolaev, E. B. Yakimov, F. Ren, S. J. Pearton, J. Kim, *J. Vac. Sci. Technol. A* **2022**, *40*, 020804.
[52] D. Nicol, Y. Oshima, J. W. Roberts, L. Penman, D. Cameron, P. R. Chalker, R. W. Martin, F. C.-P. Massabuau, *Appl. Phys. Lett.* **2023**, *122*, 062102.
[53] J. B. Varley, in *Gallium Oxide* (Eds: M. Higashiwaki, S. Fujita), Springer Series in Materials Science, Vol. *293*, Springer International Publishing, Cham **2020**, pp. 329–348.